Floquet analysis of time-averaged trapping potentials

Oliver A. D. Sandberg, Matthew T. Reeves, and Matthew J. Davis ⓘ*

ARC Centre of Excellence in Future Low-Energy Electronics Technologies (FLEET), School of Mathematics and Physics,
The University of Queensland, Brisbane, Queensland 4072, Australia

Time-averaged trapping potentials have played an important role in the development of the field of ultracold atoms. Despite their widespread application, there is not yet a complete understanding of when a system can be considered time-averaged. Here we use Floquet theory to analyze the lowest energy state of time-periodic trapping potentials, and characterize the transition from a localized state in a slowly moving trap to a delocalized state in a rapidly oscillating time-averaged potential. We investigate how the driving parameters affect the density and phase of the Floquet ground state, and provide a quantitative measure of the degree to which they can be considered time-averaged. We study a number of simple representative systems, and comment on the features affecting the experimental realization of time-averaged trapping potentials.

I. INTRODUCTION

Ultracold atomic gases provide a versatile testing ground for the study of quantum many-body physics. The ability to precisely control experimental conditions such as trapping potentials and interaction parameters allows them to be used as a toolbox for designer matter, and their relative simplicity often allows for direct comparison with theory [1]. The high degree of control and cleanliness can allow the investigation of novel phases of matter and novel far-from-equilibrium phenomena which are often not accessible in solid-state systems [2].

The flexible control and engineering of trap geometries have been important features in cold atom research, opening intriguing possibilities for quantum simulation [3], quantum computation [4], and the creation of exotic states of matter [5,6]. One approach to trap design has been the use of time-averaging: moving a trapping potential at a frequency greater than the atoms can respond to kinematically so that the effective trap is stationary with respect to the characteristic timescale of their evolution. Examples include the time orbiting potential (TOP) trap, which Petrich *et al.* used in the original quest for a Bose-Einstein condensate (BEC) [7,8], and rapidly scanned optical dipole traps [9–17]. In a similar fashion, experiments have utilized shaken optical lattices to modify effective tunneling rates between lattice sites [18–20]. Experiments generally drive the trapping potential as fast as is technically possible to ensure they are in the time-averaged regime, following a rough guideline of $\Omega \gg \omega$: that the driving frequency Ω is much faster than the frequency of the trap ω. This raises the question: what precisely are the conditions for which the time-averaging approximation is effective?

It is important to note that the effective static trap in the time-averaged limit is merely an approximation, and the system will still exhibit some dynamical features due to the driving. Experimentally this often manifests as a reduced trap lifetime and/or an inherent heating rate of the atoms [14]. It is therefore important to understand in greater detail how these features manifest, and correspondingly how they might be minimized. Some theoretical work has been done in investigating the underlying dynamical effects induced by the drive, including investigations of micromotion [21,22], but a study of the full transition from states localized in a static trap to becoming delocalized in the time-averaged limit has yet to be undertaken.

A natural approach to address these issues is Floquet theory, which provides a convenient basis in which to investigate time-periodic systems. The Floquet framework has been used in investigations of topological states [23–25], the engineering of artificial gauge fields [26,27], synthetic magnetic fields [28], spin-orbit couplings [29–31], and artificial atoms [32].

Here we apply a Floquet analysis to periodically driven trapping potentials. We examine the nature of the transition from slow driving, where the lowest energy states of the systems are localized and adiabatically follow the moving potential, to fast driving, where the lowest energy states are delocalized in the time-averaged potential. The precise way that the system couples to the drive determines how the localized to delocalized transition occurs. We provide a quantitative measure of how well the system approximates the time-averaged limit and additionally derive analytical results which give insights into the time-averaged transition.

This paper is organized as follows. In Sec. II we provide a summary of Floquet theory and a description of our numerical approach. In Sec. III we analyze a ring potential formed by a time-averaged attractive Gaussian trap. This system is both experimentally relevant [13,15–17] and relatively simple, with a Galilean transformation allowing analysis in a stationary frame. In Sec. IV, we apply our analysis to three other representative one-dimensional potentials, demonstrating key features of time-averaged systems that are important for the design and analysis of experimental setups. We highlight the different kinds of resonances that emerge for different trapping potentials. In Secs. IV A and IV B, we study

* mdavis@physics.uq.edu.au

systems which are harmonic in the time-averaged limit, so they display a collective resonance. In Sec. IV C, we study an anharmonic system, for which a collective resonance does not occur. In Sec. IV B and Sec. IV C we see the emergence of so-called "photon" resonances, which are responsible for uncontrollable heating in experimental systems [33]. Finally, we conclude in Sec. V.

II. FLOQUET THEORY

In order for this paper to be self-contained, we provide a brief overview of Floquet theory. For a more complete description we refer the reader to Refs. [34,35].

For systems with a periodic time dependence, a stationary eigenbasis does not exist. Instead, an alternative is the *stroboscopic* basis in which the states are stationary only when sampled in integer multiples of the driving period, T (frequency $\Omega = 2\pi/T$). The technique of Floquet analysis combines the usual Hilbert space of square-integrable functions, $\mathcal{R}$, with the Hilbert space of all time-periodic functions, $\mathcal{T}$, to form the composite Hilbert space $\mathcal{R} \otimes \mathcal{T}$. This composite space has norm [36]

$$\langle\langle a(t) \,|\, b(t) \rangle\rangle \equiv \frac{1}{T} \int_0^T \int a^*(x,t) b(x,t) dx \, dt, \qquad (1)$$

$$= \frac{1}{T} \int_0^T \langle a(t) \,|\, b(t) \rangle dt, \qquad (2)$$

which is a natural combination of the well-known norms of the constituent Hilbert spaces $\mathcal{R}$ and $\mathcal{T}$.

For a periodic Hamiltonian $H(t + T) = H(t)$ with period T, Floquet's theorem [37] implies that there exist so-called Floquet-state solutions to the Schrödinger equation

$$i\hbar \frac{\partial}{\partial t} \Psi(x,t) = H(x,t)\Psi(x,t), \qquad (3)$$

of the form

$$\Psi_\alpha(x,t) = e^{-i\varepsilon_\alpha t/\hbar} \Phi_\alpha(x,t), \qquad (4)$$

where $\Phi_\alpha(x,t)$ is a Floquet mode corresponding to a quasienergy ε_α. We note that, for integer n,

$$\Phi_{\alpha'}(x,t) = \Phi_\alpha(x,t)e^{in\Omega t} \equiv \Phi_{\alpha n}(x,t) \qquad (5)$$

yields an identical solution to Eq. (4) with shifted quasienergy

$$\varepsilon_\alpha \rightarrow \varepsilon_{\alpha'} = \varepsilon_\alpha + n\hbar\Omega = \varepsilon_{\alpha n}. \qquad (6)$$

Hence, the index α actually refers to a whole class of solutions indexed by $\alpha' = (\alpha, n)$, where $n = 0, \pm 1, \pm 2, \ldots$.

The quasienergies therefore, are defined modulo $\hbar\Omega$ and can be mapped into a first Brillouin zone obeying $-\hbar\Omega/2 \leqslant \varepsilon < \hbar\Omega/2$. The quasienergy can be viewed as the time-periodic analog to the quasi-momentum in Bloch's theorem of spatially periodic systems. The Floquet modes are eigenfunctions of the Floquet matrix U, which acts as a time evolution operator by stepping the solutions $\Psi_\alpha(x,t)$ forward in time by integer multiples of the driving period [35]:

$$\Psi_n(x, t + T) = \sum_m U_{nm}(T)\Psi_m(x,t). \qquad (7)$$

In this work, we construct and diagonalize the Floquet matrix to compute the Floquet states of the one-dimensional

(1D) Schrödinger equation driven by representative external potentials. While Floquet systems do not in general conserve energy, the *time-averaged* energy

$$\bar{E}_\alpha = \frac{1}{T} \int_0^T \langle \Phi_\alpha(t) \,|\, H \,|\, \Phi_\alpha(t) \rangle dt \qquad (8)$$

is conserved and may be used to classify the states; for example the Floquet "ground state" is the state with the lowest time-averaged energy.

Numerical approach

In all the cases discussed in this work, the numerical package XMDS [38] is used to simulate the Schrödinger equation

$$i\hbar \frac{\partial}{\partial t} \Psi(x,t) = \left(-\frac{\hbar^2}{2m} \frac{\partial^2}{\partial x^2} + V(x,t) \right) \Psi(x,t), \qquad (9)$$

with $V(x,t)$ a time-periodic trapping potential. We study a 1D system of length L with periodic boundary conditions. We use a basis of plane waves and use a sufficient density of grid points to ensure numerical accuracy for the Floquet states of interest (we have typically used $L = 16$ and $N = 256$ lattice points for the cases considered here).

We consider potentials of the form $V(x,t) = V_0(x - c(t))$. By varying the form of $V_0(x)$ and the driving function $c(t)$, we are able to construct a range of time-averaged potentials. To find the Floquet states as a function of the driving period $T = 2\pi/\Omega$, we simulate the time evolution of a complete basis for a time interval of one period T. From this we can construct the Floquet matrix U, which can then be diagonalized to find the Floquet states $\Phi_\alpha(x,t)$.

For driving frequencies that are near resonance with energy spacings of the bare trapping potentials it is not possible to obtain numerically accurate results. In our simulations, there are regions in which the numerics clearly do not converge, and thus the Floquet states obtained by diagonalization are not accurate. By increasing the number of lattice points, it is possible to obtain more accurate Floquet states for a greater region of parameter space, but doing so is computationally expensive. In the Floquet states computed below, the regions of nonconvergence are characterized by the states reaching the edge of the spatial grid and are correspondingly accompanied by a resonance spike in the time-averaged energy spectrum.

III. ONE-DIMENSIONAL RING POTENTIAL

We first investigate the case of a ring trap created by rapidly scanning a localized attractive potential in a circle. This geometry is common in experiments [13,14,16,17,39–41] as it may be used, for example, in matterwave interferometry [42], sensitive gravimetry [43], rotation sensing [44,45], and investigations of topological states of matter [46,47]. In particular, we investigate a system similar to that studied by Bell *et al.* [16,17] who realized a ring trap for a BEC by circularly scanning an attractive optical dipole potential. They performed a theoretical analysis of their system in order to understand unusual features in the atomic density in time-of-flight imaging, and found that it resulted from a nontrivial phase profile due to the time-averaged potential [17]. We find

that further insights are provided by applying a simple 1D Floquet analysis.

The trapping potential is

$$V(x, t) = V_D \exp\left(-\frac{(x - vt)^2}{2\sigma^2}\right), \qquad (10)$$

with $x - vt$ defined modulo L such that we have periodic boundary conditions, and $v = L/T$ is the speed of the potential such that it returns to its initial position after one driving period T. We consider an attractive potential of depth $V_D = -10$ and width $2\sigma^2 = 1$ such that $\sigma \ll L$.

Since the moving potential spends the same amount of time at each point in space in one period, the time-averaged potential is simply a constant energy offset, independent of x,

$$\bar{V}(x) = \frac{\sqrt{2\pi} V_D \sigma}{L}, \qquad (11)$$

and the Floquet states in the time-averaged limit $T \to 0$ are plane waves. Additionally, from Eq. (10), the states in the adiabatic limit $T \to \infty$ ($v \to 0$) will be the familiar eigenstates of a stationary Gaussian potential. For our parameters, there are four bound states, and a number of unbound states with winding numbers $w = 0, \pm 1, \pm 2$, etc. The winding numbers are related to the topology of the ring and are a robustly conserved quantity. In accordance with our goal of understanding the transition from these Gaussian eigenstates to the plane-wave eigenstates in the time-averaged potential, we compute the Floquet states for a range of different driving periods T.

A. The transition between time-averaged and adiabatic limits

In Fig. 1 we plot the Floquet ground state density as the scanning period T is varied. As T is increased, the Floquet ground state for the 1D ring system transitions discontinuously from an unbound, plane-wave-like state to the localized ground state of the stationary potential.

To learn more about how this transition manifests, in Fig. 1(b) we show the the time-averaged energies [Eq. (8)] and density profiles for some representative Floquet states as a function of T: shown are the ground, first-excited, and second-excited states in the adiabatic limit, and the ground state in the time-averaged limit. The energy of the bound states varies strongly with T, yet their density profiles are independent of T. In contrast, the energy of the unbound states is insensitive to the value of T and is almost constant. They also exhibit a density depletion at the instantaneous location of the attractive potential which deepens as T increases. The size of this defect is slightly different for unbound states of different winding numbers. The sharp transition between the bound and unbound Floquet ground states occurs due to an exact crossing in the energy levels at $T = 4.19$.

B. Solutions in a Galilean boosted frame

The trapping potential Eq. (10) is time-independent in the translating frame coordinates $x_c = x - vt$. This defines a Galilean boost, which transforms the Hamiltonian
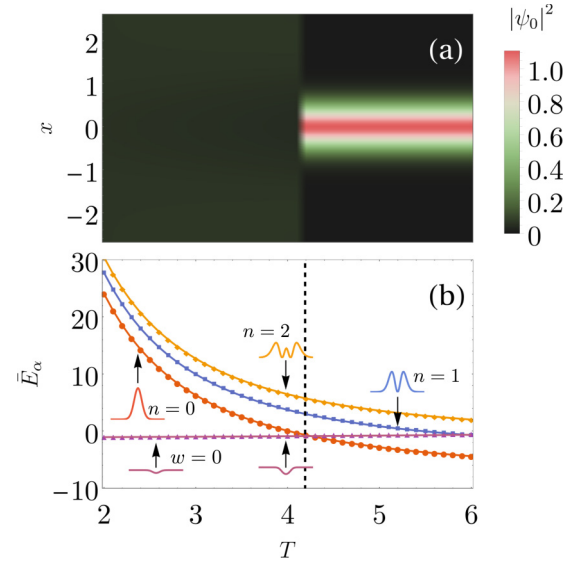

FIG. 1. Localized to delocalized transition in a 1D ring trap. (a) The Floquet ground state density at $t = 0$ for the 1D ring trap as a function of driving period. At $T = 4.19$ the ground state transitions from being homogeneous to the localized ground state of the attractive potential. (b) The time-averaged energy spectrum [Eq. (8)] as a function of driving period. Points are the results of Floquet simulations, and solid lines for the bound states labeled by quantum number n are the result of the analytic theory given by Eq. (14). The solid line for the energy of the homogeneous state with winding number $w = 0$ is from Eq. (15) with the phase given by Eq. (17). The black dashed line is the predicted transition point from equating Eqs. (14) and (17). The insets illustrate the Floquet state density corresponding to each spectral curve.

(see Appendix A)

$$H_c(x_c, t) = \frac{p^2}{2m} - vp + \frac{1}{2}mv^2 + V(x_c), \qquad (12)$$

$$= \frac{(p - mv)^2}{2m} + V(x_c). \qquad (13)$$

Since the Hamiltonian H_c is time independent, it conserves energy and we can use standard separation of variables to find solutions of the form $\Psi(x_c, t) = \varphi(x_c)e^{-iE_c t}$, where $\varphi(x_c)$ obey the eigenvalue equation $H_c\varphi(x_c) = E_c\varphi(x_c)$ and $\varphi(x_c) = \varphi(x_\ell - vt)$ are Floquet modes: after a driving period, $\varphi(x_\ell - vT) = \varphi(x_\ell - L) = \varphi(x_\ell)$, since the spatial coordinate $x_\ell - vt$ is defined modulo L. The energy in the laboratory frame E is related to the translating frame energy E_c by

$$E = E_c + v\langle p \rangle - \frac{1}{2}mv^2. \qquad (14)$$

In the regime of fast scanning, the term containing the potential evolves significantly faster than the timescale over which the kinetic term evolves. We can therefore approximate the dynamics of the system by neglecting the kinetic energy term, and obtain an analytical approximation for the wave function. Although here we consider the noninteracting case of the linear Schrödinger equation, this approach can also be applied to nonlinear Schrödinger-type equations, for example the Gross-Pitaevskii equation for a weakly interacting

Bose-Einstein condensate [17], provided the external potential energy also dominates over the interaction energy. We write the wave function in the Madelung form

$$\Psi(x_c) = \sqrt{n(x_c)}e^{i\phi(x_c)}. \tag{15}$$

where the density $n(x_c) = |\psi(x_c)|^2$ and phase $\phi(x_c)$ are both real functions. Neglecting kinetic terms and inserting Eq. (15) into the Schrödinger equation (see Appendix B) gives

$$\partial_x\phi(x_c) = \frac{V(x_c) - E'}{\hbar v}, \tag{16}$$

an ordinary differential equation for the phase, which can be readily solved to obtain

$$\phi(x_c) = \frac{V_D\sqrt{\pi}\sigma}{\sqrt{2}\hbar v}\left(\mathrm{erf}(x_c/\sqrt{2}\sigma) - \frac{2}{L}x_c\right) - \frac{2\pi w x_c}{L}, \tag{17}$$

where w is the winding number [17]. The constant

$$\begin{aligned} E' &= \frac{\sqrt{2\pi}V_D\sigma}{L} + v\frac{2\pi w\hbar}{L}, \\ &= \bar{V} + v\langle p\rangle \end{aligned} \tag{18}$$

approximates the energy of the nonkinetic terms in the boosted frame. A wave function with constant density and a phase profile given by Eq. (17) has laboratory frame energy

$$E(T) = \bar{V} + \frac{(2\pi)^2\hbar^2 w^2}{2mL^2} + \frac{\sigma T^2 V_D^2}{mL^3}\left(\frac{\sqrt{\pi}}{2} - \frac{\pi\sigma}{L}\right), \tag{19}$$

i.e., it has a constant offset $\bar{V}$, the kinetic energy of a plane-wave with $p = 2\pi\hbar w/L$, and a term which grows as T^2 which represents the contribution of the phase profile to the energy. We plot Eq. (19) as solid line in Fig. 1(b). The ground state solution has winding number zero, as this minimizes the energy.

We are now in a position to understand the behavior in Fig. 1. At $T \to \infty$ ($v = 0$), we are in the adiabatic limit, and the laboratory frame energy is the same as in the stationary problem, i.e., $E = E_c$. The bound states, which are real and nondegenerate, must have $\langle p_c\rangle = 0$ in the center-of-mass frame. That is, they have $\langle p\rangle - mv = 0$. Thus, from Eq. (14), we see that, overall, their energy changes from the stationary problem simply by the addition of the kinetic term $\frac{1}{2}mv^2$. The bound states are sensitive to the driving period T in the laboratory frame, and insensitive in the translating frame.

In contrast, from Eq. (19) it can be seen that the unbound states are quite insensitive to the drive in the laboratory frame. As $T \to \infty$, the bound states approach their translating frame energy E_c, whereas the unbound states *increase* their energy slightly due to a combination of an increasing variance σ_p as well as a growing depletion in their density profile. Hence, we have a crossover in the spectrum.

C. Quantification of time-averaging

For values of $T < 4.19$ the Floquet ground state is close to being homogeneous, but exhibits small deviations in the form of a density defect and a nonlinear phase profile that become larger as T increases. A natural question that remains is how well these states approximate the homogenous ground state in the time-averaged limit. By comparing the Floquet ground state $\psi(x, T)$ at some driving period T to the ground state of the time-averaged potential, $\psi_0(x) = L^{-1/2}$, we can
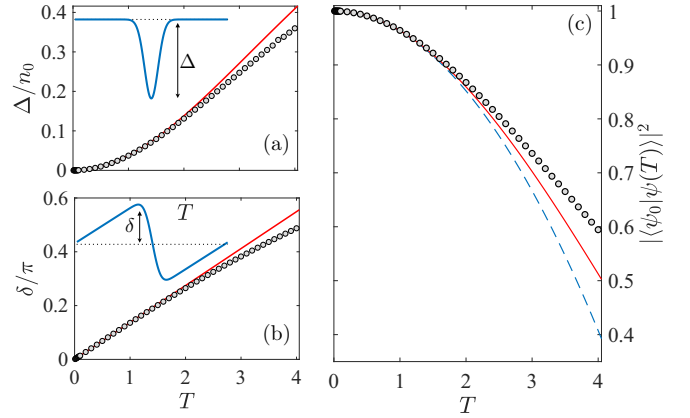

FIG. 2. Properties of the Floquet ground state vs scanning period T in the time-averaged limit $T \to 0$. (a) Depth of the density defect Δ. (b) Height of the phase defect δ. (c) Fidelity of the Floquet ground state with the $k = 0$ plane-wave ground state of the time-averaged limit. Circles show numerical results. Solid lines show the predictions given by Eq. (15). The blue dashed line in (c) shows the analytical approximation (24).

quantify the quality of the time-averaged approximation for a given period T through the fidelity $f = \langle\psi_0 | \psi(T)\rangle$. We can obtain an analytic approximation for the phase step height of the ground state as a function of driving period:

$$\delta(T) = \frac{V_D\sqrt{\pi}\sigma}{\sqrt{2}\hbar L}\left(\mathrm{erf}(x_M/\sqrt{2}\sigma) - \frac{2}{L}x_M\right)T, \tag{20}$$

where $x_M = -\sqrt{2}\sigma\sqrt{\ln(L/\sqrt{2\pi}\sigma)}$ is the x coordinate where the phase reaches its maximum value. In the inset of Fig. 2(b), we show the phase profile, along with the definition of the phase step height $\delta = \max(\phi)$.

In the boosted coordinates, the continuity equation (see Appendix B) takes the form

$$-v\,\partial_x n + \partial_x(nu) = 0, \tag{21}$$

where $u = \hbar\partial_x\phi/m$. This is an ordinary differential equation for the density $n(x)$ and can be solved to obtain

$$n(x_c) = \frac{A}{u(x_c) - v}, \tag{22}$$

where the integration constant $A = 2\pi w\hbar/mL^2 - T^{-1}$ is determined since the density must be normalized to unity. We can then obtain an expression for the depth of the density defect Δ/n_0:

$$\frac{\Delta}{n_0} = \frac{LT^2 V_D}{T^2 V_D\left(L - \sqrt{2\pi}\sigma\right) - L\hbar\left(L^2 + 2\pi Tw\right)}. \tag{23}$$

Using the full wave function $\Psi = \sqrt{n}e^{i\phi}$, we can compute the ground state fidelity as a function of T, which is shown as a solid red line in Fig. 2(c). By taking a series expansion to second order, we can obtain an analytic approximation for the fidelity with the time-averaged ground state

$$f = 1 - \frac{\pi\sigma^2 T^2 V_D^2}{L^2\hbar^2}\left(\frac{\sigma^2}{L^2} - \frac{\sigma}{\sqrt{\pi}L} + \frac{1}{12}\right), \tag{24}$$

which is plotted as a dashed blue line in Fig. 2(c).

The dip in the density and spatially varying phase profile will affect the dynamics of atoms in experimental time-averaged traps. From our 1D Floquet analysis, we are able to qualitatively reproduce the features found experimentally by Bell *et al.,* who made use of a 2D Gross-Pitaevskii simulation to investigate the phase profile of a BEC in a time-averaged ring trap [16,17]. Specifically, we find the same homogeneous Floquet states in the time-averaged limit as well as the phase profile identified as responsible for the "kink" in the ring produced in the experiment.

IV. SINUSOIDALLY DRIVEN TRAPPING POTENTIALS

While the 1D ring of Sec. III can be understood using Floquet theory, it was not necessary as there was a Galilean boost which rendered the problem time independent. Hence we could use exact diagonalization to understand the different energy dependences on T for the bound and unbound states, leading to a level crossing in the energy spectrum. However, this is only one way in which the localized to delocalized transition can occur. In this section we investigate systems for which there is no time-independent frame of reference, and so a full Floquet analysis is required. We illustrate the different ways that the Floquet states transition from the adiabatic to the time-averaged limits with three representative trapping potentials.

A. Driven harmonic oscillator

We first consider perhaps the simplest theoretical model, which breaks Galilean invariance and has ground states which are bound in both the time-averaged and adiabatic limits. We sinusoidally drive the position of a 1D harmonic oscillator

$$V(x, t) = \tfrac{1}{2}m\omega_0^2[x + A\sin(\Omega t)]^2, \qquad (25)$$

where $\Omega = 2\pi/T$ is the frequency of the drive. We choose the amplitude $A = 2$ and harmonic oscillator frequency $\omega_0 = 2\pi/1.5$ (i.e., the harmonic oscillator period is $T = 1.5$). This potential has time-average

$$\bar{V}(x) = \tfrac{1}{2}m\omega_0^2 x^2 + \tfrac{1}{4}m\omega_0^2 A^2, \qquad (26)$$

i.e, it is simply the same harmonic oscillator shifted up in energy by the constant $\tfrac{1}{4}m\omega_0^2 A^2$, as can be seen in Fig 3(a). This system will allow us to explore some additional features of Floquet systems that are important to the transition between the adiabatic and time-averaged limits.

The driven harmonic oscillator can be solved exactly by building on a solution described by Husimi [48] and requiring the solutions to obey the Floquet condition. The same results can be obtained using the harmonic potential theorem [49]. The problem can be cast as

$$i\hbar\frac{\partial}{\partial t}\psi(x, t) = [H_0 - xf(t) + q(t)]\psi(x, t), \qquad (27)$$

where $H_0 = -\hbar^2/(2m)\,\partial_x^2 + m\omega_0^2 x^2/2$ is the Hamiltonian for the unperturbed harmonic oscillator, and the time-dependent functions $f(t) = -Am\omega_0^2\sin(\Omega t)$ and $q(t) = \tfrac{1}{2}m\omega_0^2 A^2\sin^2(\Omega t)$ correspond to the driving protocol specified
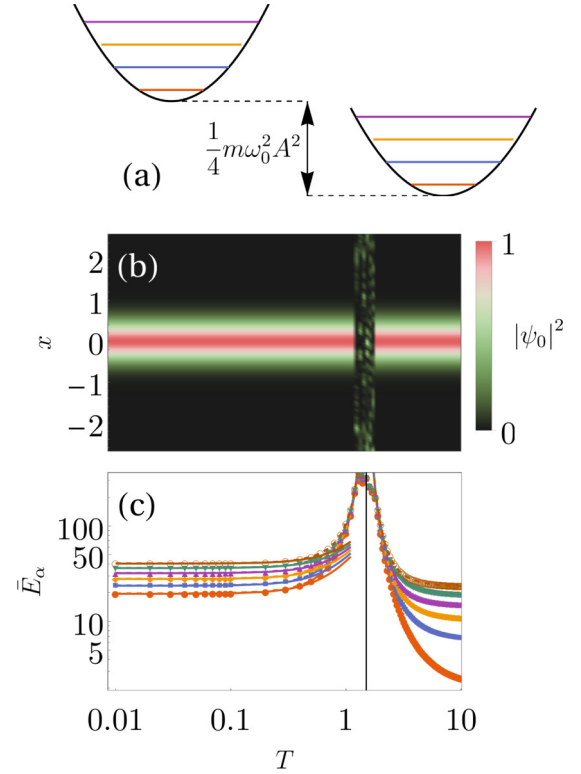

FIG. 3. Floquet analysis of the driven harmonic oscillator. (a) A schematic of the time-averaged (left) and adiabatic (right) driven harmonic oscillators, with the lowest four energies indicated. (b) The Floquet ground state density for the driven harmonic oscillator with $\omega_0 = 2\pi/1.5$. In a small region around $T_{\text{res}} = 1.5$ the strong resonance means that the numerical results for the density have not converged. Outside of this range, the numerics are stable and we obtain the expected harmonic oscillator ground state density. (c) The time-averaged energy spectrum as a function of driving period for the same parameters (markers). The analytic result Eq. (31) is shown as dashed lines. The solid lines are the result of an inverse frequency expansion to second order in T. The black vertical line at $T = 1.5$ indicates the location of the resonance.

by Eq. (25). Solutions can be written as (see Appendix C)

$$\psi_n(x, t) = \chi_n[x - \xi(t), t]$$
$$\times \exp\left[\frac{i}{\hbar}m\dot{\xi}(x - \xi) + \frac{i}{\hbar}\int_0^t \mathcal{L}(t')dt'\right], \qquad (28)$$

where $\chi_n(x)$ is a solution of the unperturbed harmonic oscillator H_0 with quantum number n. The center-of-mass coordinate is

$$\xi(t) = \frac{A\omega_0^2\sin(\Omega t)}{\Omega^2 - \omega_0^2}, \qquad (29)$$

and

$$\mathcal{L} = \tfrac{1}{2}m\dot{\xi}^2 - \tfrac{1}{2}m\omega_0^2\xi^2 + f(t)\xi - q(t) \qquad (30)$$

is the classical Lagrangian. The time-averaged energy is then given by

$$\bar{E}_n = \hbar\omega_0\left(n + \frac{1}{2}\right) + \frac{A^2 m\Omega^2\omega_0^2(\Omega^2 + \omega_0^2)}{4(\Omega^2 - \omega_0^2)^2}, \qquad (31)$$
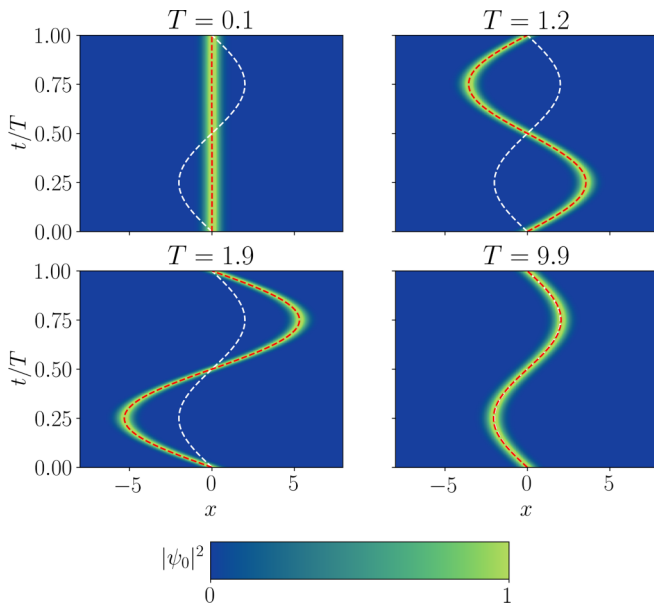
FIG. 4. Illustration of the relative motion of the Floquet ground state density and center of the trapping potential as the driving period T is increased. The red dashed line shows the analytic center-of-mass coordinate given by Eq. (29). (a) $T = 0.1$, near the time-averaged limit. (b) $T = 1.2$, just before resonance; the Floquet state undergoes large amplitude center-of-mass oscillations and is out of phase with the trapping potential. (c) $T = 1.9$, after the resonance; the Floquet state exhibits large amplitude center-of-mass oscillations and is in phase with the trapping potential. (d) $T = 9.9$, where the Floquet state is far from resonance and follows the motion of the trapping potential.

and the fidelity of the ground state is

$$f = \exp\left(-\frac{A^2 m \Omega^2 \omega_0^3}{4\hbar \left(\Omega^2 - \omega_0^2\right)^2}\right). \tag{32}$$

The results of a numerical Floquet analysis of this potential are summarized in Fig. 3. Since the energy level spacings for the harmonic oscillator are constant, a collective resonance occurs in the region of $T_{res} = 1.5$, which is clearly seen in the time-averaged energy spectrum in Fig. 3(c).

While the analytic Floquet ground state is identical for any T, numerically in a narrow region around the resonance point the energies are too high for the states to be accurately calculated by our simulation, which results in the noisy region near $T = 1.5$ in Fig. 3(b).

In Fig. 3(c), we have also plotted the results of an inverse frequency expansion [33,50–52] up to second order in T, which approximates the energy spectrum perturbatively in powers of $1/\Omega$. (For more details see Appendix D.) We find that the energy is well approximated with quadratic growth as T approaches T_{res}.

For this potential the collective resonance marks the localized to delocalized crossover. In Fig 4, for $T < T_{res}$ we can see that the Floquet ground states oscillate out of phase with the center of the potential (white dashed line), while for $T > T_{res}$ they are in phase with it. As would be expected, the effects of the driving are more significant for T close to T_{res}. For $T = 0.1$, we are clearly in the time-averaged limit, as there

is almost no center-of-mass oscillation, and the fidelity (see Fig. 7) is close to unity. In the opposite limit for $T = 9.9$ the system is close to the the adiabatic limit, and the Floquet ground state follows the oscillating potential.

In contrast to the ring potential of Sec. III, the Floquet states of the driven harmonic oscillator are the same in the two limits, so there are no energy level crossings as T is varied.

B. Driven linear potential

In the case of the driven harmonic oscillator, the Floquet states in the time-averaged and slow-moving limits were the same. This allowed us to highlight the role that the collective resonance played in the transition between the two regimes of interest. Here we consider the potential

$$V(x, t) = V_D \left| x + A \sin\left(\frac{2\pi t}{T}\right) \right|, \tag{33}$$

which is harmonic in the time-averaged limit, but has the form $V(x) \sim |x|$ in the slow-moving limit. We choose the numerical parameters $V_D = 10$ and $A = 3$. The analytic expression for the time-averaged potential is

$$\frac{\bar{V}(x)}{V_D} = \begin{cases} 2\left[\sqrt{A^2 - x^2} + x \sin^{-1}(x/A)\right]/\pi, & |x| \leqslant A, \\ |x|, & |x| > A. \end{cases} \tag{34}$$

In the time-averaged limit the Floquet states are well-approximated by harmonic oscillator eigenstates. Performing a series expansion in x gives

$$\frac{\bar{V}(x)}{V_D} \approx \frac{2A}{\pi} + \left(\frac{1}{\pi A}\right)x^2 + O(x^4) \tag{35}$$

which yields a harmonic oscillator frequency of $\omega_{HO} = (2V_D/\pi A)^{1/2}$.

In Fig. 5(b) we plot the Floquet ground state density as a function of the period T, and again observe the presence of a collective resonance peak due to the equal energy spacing of the time-averaged harmonic oscillator potential. As in the harmonic oscillator case (Sec. IV A), for $T \ll T_{res} \approx 2\pi/\omega_{HO}$ the Floquet ground state is delocalized and oscillates out of phase with the potential, and vice versa for $T \gg T_{res}$. The collective resonance is again the most significant contribution to the decrease in fidelity with increasing T and thus the transition to the adiabatic limit. A new feature for this potential, however, is the presence of multi-"photon" resonances [33], which appear as smaller resonances outside of the main resonance peak. These resonances are due to avoided crossings in the *quasienergy* spectrum as a result of hybridization of states in one "photon" block with another. In terms of the extended Hilbert space $\mathcal{H} \otimes \mathcal{T}$, an N-"photon" resonance results from the coupling of two Fourier modes k, ℓ with $k - \ell = N$ in the space $\mathcal{T}$. These resonances are not captured to any order by inverse frequency expansion, which explicitly removes the matrix elements responsible for the coupling of one "photon" block to another, dealing only with diagonal elements in the extended space. These resonances are important for experiments, as they result in a breakdown of adiabatic following [53] of the Floquet states and physically represent heating due to energy transferred from the drive [33]. Thus, experiments
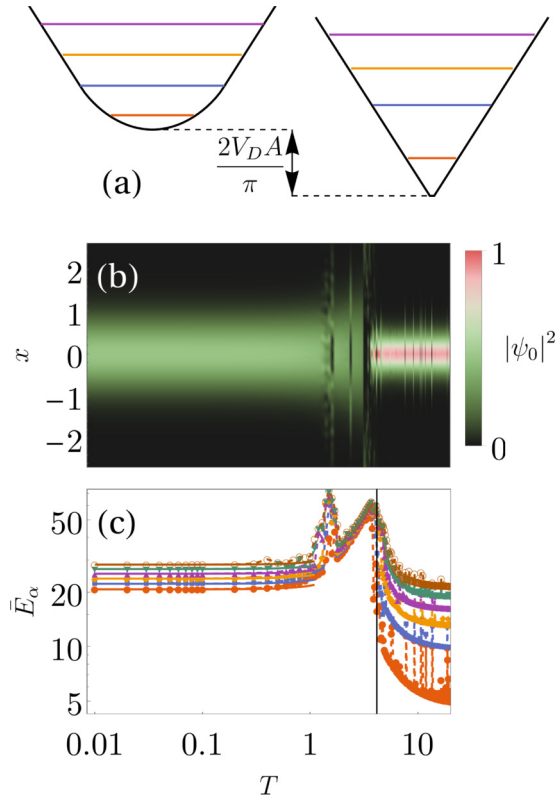
FIG. 5. Large collective resonance and emergence of "photon" resonances for the driven $|x|$ potential. (a) A schematic of the time-averaged (left) and adiabatic (right) driven $|x|$ potential, with the lowest four energies indicated. (b) The Floquet ground state density for the driven $|x|$ potential as a function of driving period T. (c) The time-averaged energy spectrum for the driven $|x|$ potential as a function of driving period T. The states undergo a collective resonance, the position of which can be predicted by the energy spacings for low T (vertical black line). The numerics do not converge in small regions around the collective and photon resonance points where the Floquet state reaches the edge of the x grid. Solid lines are the result of an inverse frequency expansion, where the third order term has been fitted to the Floquet simulation.

should choose parameters which avoid this breakdown for preparing and measuring time-periodic systems.

This behavior is related to the more general phenomenon of Floquet prethermalization in nonintegrable systems, wherein states thermalize (in the sense of the eigenstate thermalization hypothesis (ETH) [54–56]) to a quasistable state according to a Hamiltonian that does not govern its evolution [57]. This results in two separate timescales: a heating time τ_h and a relaxation time, which here depends on how quickly the system can relax to a prethermal state under the effective (local) Hamiltonian H_{eff}, which is expected to obey the usual ETH. The state will only relax to an equilibrium state of H_{eff} if the relaxation time is much shorter than τ_h. Periodically driven systems are in some sense useful only to the extent that the system can be made to prethermalize under H_{eff} [58].

A periodic drive can resonantly create excitations within a low-energy subspace [59] via "photon" resonances. In the small-T limit, the coupling matrix elements are generally suppressed, and a prethermal state persists for an exponentially long time [33,60], before heating up to infinite temperature as predicted by the Floquet ETH. This may provide an explanation for why we do not see photon resonance effects for small values of T.

In addition, systems which are integrable or display many-body localization do not obey the Floquet ETH and thus do not heat up to an infinite temperature state. Hence, the harmonic oscillator described in Sec. IV A does not display resonances and will not undergo heating.

C. Driven quartic double well

The previous two trapping potentials considered in this section have had harmonic oscillator eigenfunctions in the time-averaged limit. This led to a collective resonance occurring and a clear separation between localized and delocalized regimes. Here we consider a trapping potential which still admits bound states in both the time-averaged and slow-moving limits, but has an anharmonic spectrum everywhere.

We consider the quartic double-well potential and subject it to sinusoidal driving,

$$V(x', t) = A\left(e_0 x'^4 - x'^2\right), \tag{36}$$

where the coordinate $x' = x + \epsilon \sin(\Omega t)$, and we choose the numerical values $A = 1.5$ and $e_0 = 0.36$, so that the potential has a double-well shape in the adiabatic limit. This potential Eq. (36) has time-average

$$\bar{V}(x) = A\left(e_0 x^4 + \tfrac{1}{8}\epsilon^2(3e_0\epsilon^2 - 4) + x^2(3e_0\epsilon^2 - 1)\right). \tag{37}$$

The results for this potential are summarized in Fig. 6, where it can be seen that this system transitions in a manner qualitatively different from the previous two. Since there is no collective resonance, there is no single point after which the states become localized in the potential. The Floquet ground state density as a function of the driving period T is shown in Fig. 6(b). A number of different ground states densities are apparent, and there are regions of collective resonances, photon resonances, and mixing between the states of each limit. Since the energy level spacings of the lowest energy states are reasonably similar in magnitude, there is a quasi-collective resonance where many of the states are destroyed at similar values of T. As before, it is possible to compute an approximation to the high frequency energy spectrum via an inverse frequency expansion, and we find good agreement at second order [solid lines in Fig. 6(c)].

D. Behaviour of fidelity

For the harmonic systems considered in Secs. IV A and IV B, which have equal energy level spacings in the time-averaged limit, a collective resonance marks the localized to delocalized transition point. For anharmonic systems as in Sec. IV C, this collective resonance does not occur and, as such, there is no clear localized to delocalized transition point and states are able to undergo mixing in intermediate regions of parameter space.

In Secs. IV B and IV C, we highlighted the impact of so-called "photon" resonances on the transition and general dynamics of Floquet systems. For experiments, regions of
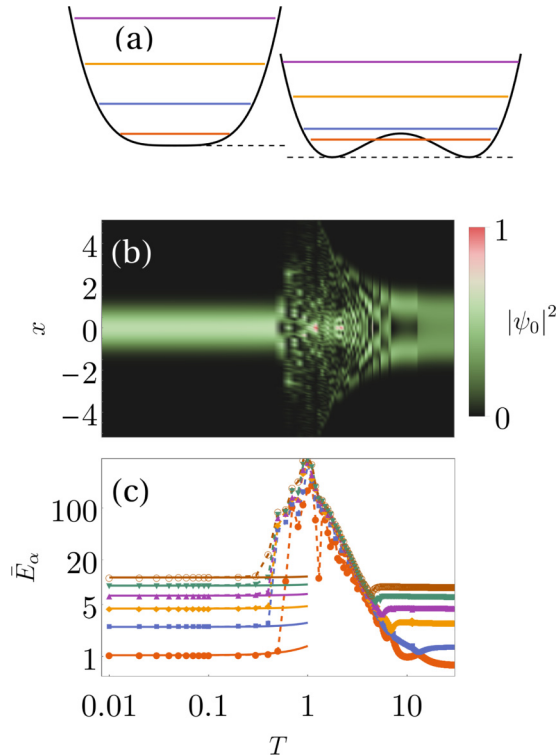
FIG. 6. The quartic double well displays a quasicollective resonance as well as photon resonances. (a) The time-averaged (left) and adiabatic (right) potentials. (b) The density of the Floquet ground state for the driven double well potential as a function of T. At large T we recover the two-peaked ground state of the double-well potential. (c) The time-averaged energy spectrum for the driven double-well potential as a function of T. The numerics do not converge in regions where the Floquet state reaches the edge of the x grid. Solid lines are the result of an inverse frequency expansion to third order.

photon resonance should be avoided, as it leads to uncontrollable heating which will ultimately destroy the system.

The fidelity between the time-averaged ground state provides a quantitative measure of the degree to which a Floquet state is in the time-averaged limit. In Fig. 7 we plot the fidelity as a function of scaled driving period T/T_0, where the characteristic driving period $T_0 = h/\Delta E$ is determined by the energy difference ΔE between the ground and first excited states. The fidelity decay for the Floquet systems studied is well approximated by a Gaussian (solid lines in Fig. 7). For the quartic double well, the fidelity remains close to unity until a photon resonance sharply destroys the Floquet ground state.

V. CONCLUSIONS

We have studied time-averaged potentials for ultracold atoms using the method of Floquet analysis. We first considered a 1D ring potential formed by an attractive Gaussian beam scanned at a constant velocity. Due to the Galilean invariance of this potential, it was possible to obtain Floquet states for this system by transforming to a time-independent
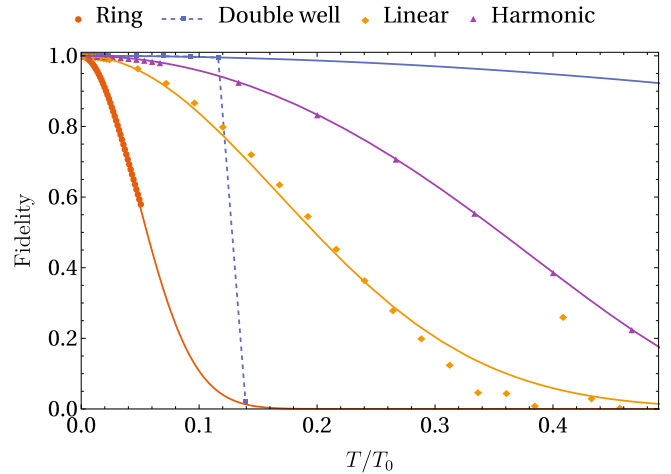

FIG. 7. Comparison of the fidelity of the Floquet ground state with the time-averaged limit for as a function of scaled driving period for the three potentials considered in this section. Solid lines are a Gaussian fit to the data, with the exception of the harmonic oscillator case, which uses the analytic fidelity given by Eq. (32). Dashed lines have been added between the quartic double-well data points to aid the eye.

frame of reference. We have built on the earlier work of Bell *et al.* [17] to demonstrate how the Floquet states of this system change as a function of the driving period, and have derived several approximate analytic results. Our results provide further insights into the nature of this time-averaged potential.

We then performed a Floquet analysis of three other 1D potentials where the position of the trap was driven sinusoidally. These examples illustrated the effects of a collective resonance when harmonic oscillator potentials were driven near their resonant frequency, and photon-resonance effects due to coupling between individual Floquet states. We performed an analytic inverse-frequency expansion in the fast-moving limit that agreed well with our numerical results. We used the fidelity to provide a quantitative measure of the degree to which these systems approximated the time-averaged limit.

Our results clearly illustrate the transition of the ground state density from adiabatic following of a moving potential to being delocalized in the time-averaged potential. They show the resonances that can lead to heating that when making use of of driven trapping potentials for ultracold atoms.

The fidelity between the time-averaged state and the Floquet states decays proportionally to T^2 for small T and is approximately Gaussian at larger T. This fidelity decay is a common feature of all the systems studied here and provides a more quantitative means for determining an appropriate scanning rate than the rule of thumb $\Omega \gg \omega$.

In this work, we restricted ourselves to potentials which are monochromatically driven in time, which have a single frequency of driving. For nonmonochromatic driving, the presence of multiple driving frequencies drastically increases the complexity of the resulting dynamics, and as such is an important consideration for future work.

APPENDIX A: GALILEAN TRANSFORMATION TO A TIME-INDEPENDENT HAMILTONIAN

The Schrödinger equation is

$$i\hbar\frac{\partial \Psi_\ell(x_\ell,t)}{\partial t} = \underbrace{\left[-\frac{\hbar}{2m}\frac{\partial^2}{\partial x_\ell^2} + V(x_\ell,t)\right]}_{H(x_\ell,t)}\Psi_\ell(x_\ell,t), \quad \text{(A1)}$$

where $\Psi_\ell(x_\ell,t)$ is the wave function in the laboratory frame and x_ℓ is the laboratory frame position coordinate.

The coordinate transformation to the moving frame,

$$x_c = x_\ell - vt, \quad \text{(A2)}$$

transforms the various functions according to

$$\Psi_\ell(x_\ell) = \Psi_\ell(x_c + vt), \quad \text{(A3)}$$

$$\frac{\partial}{\partial t}\Psi_\ell(x_\ell,t) = \frac{\partial}{\partial t}\Psi_\ell(x_c + vt, t) - v\frac{\partial}{\partial x_c}\Psi_\ell(x_c + vt, t), \quad \text{(A4)}$$

$$\frac{\partial}{\partial x_\ell}\Psi_\ell(x_\ell,t) = \frac{\partial}{\partial x_c}\Psi_\ell(x_c + vt, t), \quad \text{(A5)}$$

so that Eq. (A1) becomes

$$i\hbar\frac{\partial}{\partial t}\Psi_\ell = \underbrace{\left[-\frac{\hbar^2}{2m}\frac{\partial^2}{\partial x_c^2} + i\hbar v\frac{\partial}{\partial x_c} + V(x_c + vt, t)\right]}_{H'(x_c,t)}\Psi_\ell. \quad \text{(A6)}$$

Now recall that $\frac{\partial}{\partial x_c} = ip$, where $p = \hbar k$ is the conjugate momentum, and we can write

$$i\hbar\frac{\partial}{\partial t}\Psi_\ell = \left[\frac{p^2}{2m} - vp + V(x_c + vt, t)\right]\Psi_\ell. \quad \text{(A7)}$$

Since the potential is of the form $V(x,t) = V(x - vt)$, the Hamiltonian becomes time independent and can be solved via separation of variables, giving the eigenvalue equation

$$\left[\frac{p_c^2}{2m} - vp_c + V(x_c)\right]\varphi(x_c) = E'\varphi(x_c). \quad \text{(A8)}$$

The bound state solutions of this eigenvalue problem (which move with the potential in the laboratory frame) have $\langle p \rangle = mv$. In the moving frame, they have $\langle p_c \rangle = 0$, i.e., $p_c = p - mv$. So the Hamiltonian in the moving frame (in terms of the laboratory momenta) is

$$H_c = \frac{(p - mv)^2}{2m} + V(x_c), \quad \text{(A9)}$$

which is simply $H' + \frac{1}{2}mv^2$. Since the addition of a constant does not change the dynamics, we can solve the moving frame problem given by Eq. (A9).

APPENDIX B: MADELUNG TRANSFORMATION FOR A BOOSTED HAMILTONIAN

Inserting the Madelung form $\varphi(x_c) = \sqrt{n(x_c)}e^{i\phi(x_c)}$ into Eq. (A8) and equating the imaginary components yields

$$-v\,\partial_x n(x) + \partial_x[n(x)u(x)] = 0, \quad \text{(B1)}$$

where $u(x) = \hbar/m\,\partial_x\phi(x)$. Equating the real parts gives

$$V(x) - E' - mvu + \frac{1}{2}mu^2 - \frac{\hbar^2}{2m}\frac{\partial_x^2\sqrt{n}}{\sqrt{n}} = 0, \quad \text{(B2)}$$

where E' is a constant independent of x. We assume $V \gg \frac{1}{2}mu^2$, $\frac{\hbar^2}{2m}\frac{\partial_x^2\sqrt{n}}{\sqrt{n(x}}$ to obtain

$$\partial_x\phi(x) = \frac{V(x) - E'}{\hbar v}. \quad \text{(B3)}$$

APPENDIX C: DRIVEN HARMONIC OSCILLATOR SOLUTION

We consider a harmonic trap with frequency ω_0 and subject it to driving which can depend linearly on x and arbitrarily on t:

$$i\hbar\frac{\partial}{\partial t}\psi(x,t) = [H_0 - xf(t) + q(t)]\psi(x,t), \quad \text{(C1)}$$

where

$$H_0 = -\frac{\hbar^2}{2m}\frac{\partial^2}{\partial x^2} + \frac{1}{2}m\omega_0^2 x^2 \quad \text{(C2)}$$

is the Hamiltonian of the unperturbed harmonic oscillator. A related problem was described by Husimi [48] without the time-dependent function $q(t)$.

We proceed by performing a coordinate transformation $x' = x - \xi(t)$, where ξ is a function of time to be specified below. The Schrödinger equation is then

$$i\hbar\frac{\partial}{\partial t}\psi(x' + \xi, t) = \left[i\hbar\dot{\xi}\frac{\partial}{\partial x'} - \frac{\hbar^2}{2m}\frac{\partial^2}{\partial x'^2} + \frac{1}{2}m\omega_0^2(x' + \xi)^2 \right.$$
$$\left. - (x' + \xi)f(t) + q(t)\right]\psi(x' + \xi, t). \quad \text{(C3)}$$

We write the solution in terms of a phase and an arbitrary function $\varphi(x' + \xi, t)$:

$$\psi(x' + \xi, t) = \exp\left(\frac{i}{\hbar}m\dot{\xi}x'\right)\varphi(x' + \xi, t), \quad \text{(C4)}$$

and insert this into (C3) to obtain

$$i\hbar\frac{\partial}{\partial t}\varphi(x' + \xi, t)$$
$$= \left(-\frac{\hbar^2}{2m}\frac{\partial^2}{\partial x'^2} + \frac{1}{2}m\omega_0^2 x'^2\right)\varphi(x' + \xi, t)$$
$$+ \left(-f(t) + m\omega_0^2\xi + m\ddot{\xi}\right)x'\varphi(x' + \xi, t)$$
$$+ \left(q(t) - f(t)\xi + \frac{m}{2}\omega_0^2\xi^2 - \frac{m}{2}\dot{\xi}^2\right)\varphi(x' + \xi, t). \quad \text{(C5)}$$

Requiring that

$$f(t) - m\omega_0^2\xi - m\ddot{\xi} = 0 \quad \text{(C6)}$$

eliminates the second line of Eq. (C5). The term in brackets on the third line, which depends only on time, can be eliminated by performing a further transformation

$$\varphi = \chi \exp\left(\frac{i}{\hbar}\int_0^t f(t')\xi - q(t') + \frac{1}{2}m\dot{\xi}^2 - \frac{1}{2}m\omega_0^2\xi^2 dt'\right),$$
(C7)

so that the full solution is

$$\psi(x,t) = \chi_n[x - \xi(t), t]$$

$$\times \exp\left(\frac{i}{\hbar}m\dot{\xi}(x - \xi) + \frac{i}{\hbar}\int_0^t \mathcal{L}(t')dt'\right), \quad \text{(C8)}$$

where $\chi_n[x - \xi(t)]$ are the usual harmonic oscillator wave functions with center-of-mass coordinate ξ and

$$\mathcal{L} = \frac{1}{2}m\dot{\xi}^2 - \frac{1}{2}m\omega_0^2\xi^2 + f(t)\xi - q(t) \quad \text{(C9)}$$

is the classical Lagrangian. For the potential given by Eq. (25), we can identify $f(t) = -Am\omega_0^2\sin(\Omega t)$ and solve Eq. (C6). We take $\xi(0) = 0$ and, crucially, include the Floquet condition $\dot{\xi}(0) = \dot{\xi}(T)$. The solution is then

$$\xi(t) = \frac{A\omega_0^2\sin(\Omega t)}{\Omega^2 - \omega_0^2}. \quad \text{(C10)}$$

We can additionally identify $q(t) = \frac{1}{2}m\omega_0^2 A^2\sin^2(\Omega t)$ and compute the integral of the classical Lagrangian Eq. (30). From the full wave functions we can compute the energy as a function of time:

$$E_n(t) = \hbar\omega_0\left(n + \frac{1}{2}\right)$$

$$+ \frac{A^2m\Omega^2\omega_0^2\left(\Omega^2\sin^2(\Omega t) + \omega_0^2\cos^2(\Omega t)\right)}{2\left(\Omega^2 - \omega_0^2\right)^2} \quad \text{(C11)}$$

which has time-average

$$\bar{E}_n = \hbar\omega_0\left(n + \frac{1}{2}\right) + \frac{A^2m\Omega^2\omega_0^2\left(\Omega^2 + \omega_0^2\right)}{4\left(\Omega^2 - \omega_0^2\right)^2}. \quad \text{(C12)}$$

APPENDIX D: INVERSE FREQUENCY EXPANSION

Here we outline the calculation for the inverse frequency expansion for the driven harmonic oscillator. We follow Ref. [51], although we note that the same result may be obtained with equivalent methods described in Refs. [33,50,52].

The effective Hamiltonian given in [51] is

$$H_{\text{eff}}^{(0)} = H_0, \quad \text{(D1)}$$

$$H_{\text{eff}}^{(1)} = \frac{1}{\Omega}\sum_{j=1}^\infty \frac{1}{j}\left[V^{(j)}, V^{(-j)}\right], \quad \text{(D2)}$$

$$H_{\text{eff}}^{(2)} = \frac{1}{2\Omega^2}\sum_{j=1}^\infty ([[V^{(j)}, H_0], V^{(-j)}] + [[V^{(-j)}, H_0], V^{(j)}),$$
(D3)

where H_0 is the time-averaged Hamiltonian and $V^{(j)}$ are the Fourier components of the driving potential. Recall the Hamiltonian for the driven harmonic oscillator is

$$H(x,t) = \frac{p^2}{2m} + \frac{1}{2}m\omega_0^2[x + A\sin(\Omega t)]^2, \quad \text{(D4)}$$

and the time-averaged Hamiltonian is

$$H_0 = \frac{p^2}{2m} + \frac{1}{2}m\omega_0^2 x^2 + \frac{1}{4}m\omega_0^2 A^2. \quad \text{(D5)}$$

The Fourier components of the potential are

$$V^{(0)} = \frac{1}{2}m\omega_0^2 x^2 + \frac{1}{4}m\omega_0^2 A^2, \quad \text{(D6)}$$

$$V^{(1)} = -\frac{1}{2}iAxm\omega_0^2 = -V^{(-1)}, \quad \text{(D7)}$$

$$V^{(2)} = -\frac{1}{8}A^2m\omega_0^2 = V^{(-2)}. \quad \text{(D8)}$$

We immediately see that $H_{\text{eff}}^{(1)} = 0$, since $|V^{(-j)}| = |V^{(j)}|$. Computing the commutators, we find that the second-order term is

$$H_{\text{eff}}^{(2)} = \frac{A^2m\omega_0^4}{4\Omega^2}. \quad \text{(D9)}$$

Thus, to second order, we have

$$H_{\text{eff}} = \frac{p^2}{2m} + \frac{1}{2}m\omega_0^2 x^2 + \frac{1}{4}m\omega_0^2 A^2 + \frac{A^2m\omega_0^4}{4\Omega^2}, \quad \text{(D10)}$$

which gives a quasienergy spectrum

$$\varepsilon_\alpha = \left(\alpha + \frac{1}{2}\right)\hbar\omega_0 + \frac{1}{4}m\omega_0^2 A^2 + \frac{A^2m\omega_0^4}{4\Omega^2}. \quad \text{(D11)}$$

The time-averaged energy can be given in terms of the quasienergy by using the Hellmann-Feynman theorem [34,61],

$$\bar{E}_\alpha = \varepsilon_\alpha - \Omega\frac{\partial\varepsilon_\alpha}{\partial\Omega}, \quad \text{(D12)}$$

and we finally obtain the expression for the time-averaged energy to second order:

$$\bar{E}_\alpha = \left(\alpha + \frac{1}{2}\right)\hbar\omega_0 + \frac{1}{4}m\omega_0^2 A^2 + \frac{3A^2m\omega_0^4}{4\Omega^2}. \quad \text{(D13)}$$

We note that this agrees exactly with Eq. (C12) expanded to second order in $1/\Omega$.

[1] N. Goldman, J. C. Budich, and P. Zoller, Topological quantum matter with ultracold gases in optical lattices, Nat. Phys. **12**, 639 (2016).

[2] M. T. Manzoni, L. Mathey, and D. E. Chang, Designing exotic many-body states of atomic spin and motion in photonic crystals, Nat. Commun. **8**, 14696 (2017).

[3] I. Bloch, J. Dalibard, and S. Nascimbène, Quantum simulations with ultracold quantum gases, Nat. Phys. **8**, 267 (2012).

[4] C. Zipkes, S. Palzer, C. Sias, and M. Köhl, A trapped single ion inside a Bose-Einstein condensate, Nature (London) **464**, 388 (2010).

[5] M. Greiner, O. Mandel, T. Rom, A. Altmeyer, A. Widera, T. W. Hänsch, and I. Bloch, Quantum phase transition from a superfluid to a Mott insulator in an ultracold gas of atoms, Nature (London) **415**, 39 (2002).

[6] J. R. Li, J. Lee, W. Huang, S. Burchesky, B. Shteynas, F. Ç. Topi, A. O. Jamison, and W. Ketterle, A stripe phase with supersolid properties in spin-orbit-coupled Bose-Einstein condensates, Nature (London) **543**, 91 (2017).

[7] W. Petrich, M. H. Anderson, J. R. Ensher, and E. A. Cornell, Stable, Tightly Confining Magnetic Trap for Evaporative Cooling of Neutral Atoms, Phys. Rev. Lett. **74**, 3352 (1995).

[8] D. J. Han, R. H. Wynar, Ph. Courteille, and D. J. Heinzen, Bose-Einstein condensation of large numbers of atoms in a magnetic time-averaged orbiting potential trap, Phys. Rev. A **57**, R4114(R) (1998).

[9] N. Friedman, L. Khaykovich, R. Ozeri, and N. Davidson, Compression of cold atoms to very high densities in a rotating-beam blue-detuned optical trap, Phys. Rev. A **61**, 031403(R) (2000).

[10] V. Milner, J. L. Hanssen, W. C. Campbell, and M. G. Raizen, Optical Billiards for Atoms, Phys. Rev. Lett. **86**, 1514 (2001).

[11] P. Rudy, R. Ejnisman, A. Rahman, S. Lee, and N. Bigelow, An all optical dynamical dark trap for neutral atoms, Opt. Express **8**, 159 (2009).

[12] S. K. Schnelle, E. D. van Ooijen, M. J. Davis, N. R. Heckenberg, and H. Rubinsztein-Dunlop, Versatile two-dimensional potentials for ultra-cold atoms, Opt. Express **16**, 1405 (2008).

[13] K. Henderson, C. Ryu, C. MacCormick, and M. G. Boshier, Experimental demonstration of painting arbitrary and dynamic potentials for Bose-Einstein condensates, New J. Phys. **11**, 043030 (2009).

[14] M. Gildemeister, E. Nugent, B. E. Sherlock, M. Kubasik, B. T. Sheard, and C. J. Foot, Trapping ultracold atoms in a time-averaged adiabatic potential, Phys. Rev. A **81**, 031402(R) (2010).

[15] B. E. Sherlock, M. Gildemeister, E. Owen, E. Nugent, and C. J. Foot, Time-averaged adiabatic ring potential for ultracold atoms, Phys. Rev. A **83**, 043408 (2011).

[16] T. A. Bell, J. A. P. Glidden, L. Humbert, M. W. J. Bromley, S. A. Haine, M. J. Davis, T. W. Neely, M. A. Baker, and H. Rubinsztein-Dunlop, Bose-Einstein condensation in large time-averaged optical ring potentials, New J. Phys. **18**, 035003 (2016).

[17] T. A. Bell, G. Gauthier, T. W. Neely, H. Rubinsztein-Dunlop, M. J. Davis, and M. A. Baker, Phase and micromotion of Bose-Einstein condensates in a time-averaged ring trap, Phys. Rev. A **98**, 013604 (2018).

[18] H. Lignier, C. Sias, D. Ciampini, Y. Singh, A. Zenesini, O. Morsch, and E. Arimondo, Dynamical Control of Matter-Wave Tunneling in Periodic Potentials, Phys. Rev. Lett. **99**, 220403 (2007).

[19] C. Sias, H. Lignier, Y. P. Singh, A. Zenesini, D. Ciampini, O. Morsch, and E. Arimondo, Observation of Photon-Assisted Tunneling in Optical Lattices, Phys. Rev. Lett. **100**, 040404 (2008).

[20] C. E. Creffield, F. Sols, D. Ciampini, O. Morsch, and E. Arimondo, Expansion of matter waves in static and driven periodic potentials, Phys. Rev. A **82**, 035601 (2010).

[21] J. H. Müller, O. Morsch, D. Ciampini, M. Anderlini, R. Mannella, and E. Arimondo, Atomic Micromotion and Geometric Forces in a Triaxial Magnetic Trap, Phys. Rev. Lett. **85**, 4454 (2000).

[22] K. J. Challis, R. J. Ballagh, and C. W. Gardiner, Solitary-wave description of condensate micromotion in a time-averaged orbiting potential trap, Phys. Rev. A **70**, 053605 (2004).

[23] M. C. Rechtsman, J. M. Zeuner, Y. Plotnik, Y. Lumer, D. Podolsky, F. Dreisow, S. Nolte, M. Segev, and A. Szameit, Photonic Floquet topological insulators, Nature (London) **496**, 196 (2013).

[24] T. Mikami, S. Kitamura, K. Yasuda, N. Tsuji, T. Oka, and H. Aoki, Brillouin-Wigner theory for high-frequency expansion in periodically driven systems: Application to Floquet topological insulators, Phys. Rev. B **93**, 144307 (2016).

[25] B. G. Swingle and T. A. B. Kennedy, Generation of topological flows by phase imprinting, J. Phys. B: At. Mol. Opt. Phys. **38**, 3503 (2005).

[26] T. Kuwahara, T. Mori, and K. Saito, Floquet-Magnus theory and generic transient dynamics in periodically driven many-body quantum systems, Ann. Phys. (N.Y). **367**, 96 (2016).

[27] J. Dalibard and F. Gerbier, Colloquium: Artificial gauge potentials for neutral atoms, Rev. Mod. Phys. **83**, 1523 (2011).

[28] C. E. Creffield, G. Pieplow, F. Sols, and N. Goldman, Realization of uniform synthetic magnetic fields by periodically shaking an optical square lattice, New J. Phys. **18**, 093013 (2016).

[29] B. H. Wu and J. C. Cao, Time-dependent multimode transport through quantum wires with spin-orbit interaction: Floquet scattering matrix approach, Phys. Rev. B **73**, 245412 (2006).

[30] Z. Z. Li, C. H. Lam, and J. Q. You, Floquet engineering of long-range p -wave superconductivity: Beyond the high-frequency limit, Phys. Rev. B **96**, 155438 (2017).

[31] A. López, Z. Z. Sun, and J. Schliemann, Floquet spin states in graphene under ac-driven spin-orbit interaction, Phys. Rev. B **85**, 205428 (2012).

[32] C. Deng, J. Orgiazzi, F. Shen, S. Ashhab, and A. Lupascu, Observation of Floquet States in a Strongly Driven Artificial Atom, Phys. Rev. Lett. **115**, 133601 (2015).

[33] A. Eckardt and E. Anisimovas, High-frequency approximation for periodically driven quantum systems from a Floquet-space perspective, New J. Phys. **17**, 093039 (2015).

[34] M. Grifoni and P. Hänggi, Driven quantum tunneling, Phys. Rep. **304**, 229 (1998).

[35] L. E. Reichl, *Nonlinear Dynamics* (Springer, New York, 1992), pp. 384–387.

[36] H. Sambe, Steady states and quasienergies of a quantum-mechanical system in an oscillating field, Phys. Rev. A **7**, 2203 (1973).

[37] G. Floquet, Sur les équations différentielles linéaires à coefficients périodiques, Ann. Sci. l'École Norm. Supérieure **12**, 47 (1883).

[38] G. R. Dennis, J. J. Hope, and M. T. Johnsson, XMDS2: Fast, scalable simulation of coupled stochastic partial differential equations, Comput. Phys. Commun. **184**, 201 (2013).

[39] I. Lesanovsky and W. Von Klitzing, Time-Averaged Adiabatic Potentials: Versatile Matter-Wave Guides and Atom Traps, Phys. Rev. Lett. **99**, 083001 (2007).

[40] M. Gildemeister, Trapping ultracold atoms in time-averaged adiabatic potentials, Ph.D. thesis, University of Oxford, 2009, https://ora.ox.ac.uk/objects/uuid:0572480a-9114-426e-b853-b6be30c7594e.

[41] S. Pandey, H. Mas, G. Drougakis, P. Thekkeppatt, V. Bolpasi, G. Vasilakis, K. Poulios, and W. von Klitzing, Hypersonic Bose-Einstein condensates in accelerator rings, Nature (London) **570**, 205 (2019).

[42] E. J. Su, S. Wu, and M. G. Prentiss, Atom interferometry using wave packets with constant spatial displacements, Phys. Rev. A **81**, 043631 (2010).

[43] B. Canuel, F. Leduc, D. Holleville, A. Gauguet, J. Fils, A. Virdis, A. Clairon, N. Dimarcq, Ch. J. Bordé, A. Landragin, and P. Bouyer, Six-Axis Inertial Sensor Using Cold-Atom Interferometry, Phys. Rev. Lett. **97**, 010402 (2006).

[44] T. L. Gustavson, P. Bouyer, and M. A. Kasevich, Precision Rotation Measurements with an Atom Interferometer Gyroscope, Phys. Rev. Lett. **78**, 2046 (1997).

[45] S. Wu, E. Su, and M. Prentiss, Demonstration of an Area-Enclosing Guided-Atom Interferometer for Rotation Sensing, Phys. Rev. Lett. **99**, 173201 (2007).

[46] O. Morizot, Y. Colombe, V. Lorent, H. Perrin, and B. M. Garraway, Ring trap for ultracold atoms, Phys. Rev. A **74**, 023617 (2006).

[47] S. Yao, Z. Yan, and Z. Wang, Topological invariants of Floquet systems: General formulation, special properties, and Floquet topological defects, Phys. Rev. B **96**, 195303 (2017).

[48] K. Husimi, Miscellanea in elementary quantum mechanics, II, Prog. Theor. Phys. **9**, 381 (1953).

[49] J. F. Dobson, Harmonic-Potential Theorem: Implications for Approximate Many-Body Theories, Phys. Rev. Lett. **73**, 2244 (1994).

[50] S. Rahav, I. Gilary, and S. Fishman, Time Independent Description of Rapidly Oscillating Potentials, Phys. Rev. Lett. **91**, 110404 (2003).

[51] N. Goldman and J. Dalibard, Periodically Driven Quantum Systems: Effective Hamiltonians and Engineered Gauge Fields, Phys. Rev. X **4**, 031027 (2014).

[52] A. P. Itin and M. I. Katsnelson, Effective Hamiltonians for Rapidly Driven Many-Body Lattice Systems: Induced Exchange Interactions and Density-Dependent Hoppings, Phys. Rev. Lett. **115**, 075301 (2015).

[53] D. W. Hone, R. Ketzmerick, and W. Kohn, Time-dependent Floquet theory and absence of an adiabatic limit, Phys. Rev. A **56**, 4045 (1997).

[54] J. M. Deutsch, Quantum statistical mechanics in a closed system, Phys. Rev. A **43**, 2046 (1991).

[55] M. Srednicki, Chaos and quantum thermalization, Phys. Rev. E **50**, 888 (1994).

[56] M. Rigol, V. Dunjko, and M. Olshanii, Thermalization and its mechanism for generic isolated quantum systems, Nature (London) **452**, 854 (2008).

[57] D. Abanin, W. De Roeck, W. W. Ho, and F. Huveneers, A rigorous theory of many-body prethermalization for periodically driven and closed quantum systems, Commun. Math. Phys. **354**, 809 (2017).

[58] K. Singh, C. J. Fujiwara, Z. A. Geiger, E. Q. Simmons, M. Lipatov, A. Cao, P. Dotti, S. V. Rajagopal, R. Senaratne, T. Shimasaki, M. Heyl, A. Eckardt, and D. M. Weld, Quantifying and Controlling Prethermal Nonergodicity in Interacting Floquet Matter, Phys. Rev. X **9**, 041021 (2019).

[59] G. Sun and A. Eckardt, Optimal frequency window for Floquet engineering in optical lattices, Phys. Rev. Research **2**, 013241 (2020).

[60] T. Mori, T. N. Ikeda, E. Kaminishi, and M. Ueda, Thermalization and prethermalization in isolated quantum systems: A theoretical overview, J. Phys. B: At. Mol. Opt. Phys. **51**, 112001 (2018).

[61] B. Ya. Zeldovich, The quasienergy of a quantum mechanical system subjected to a periodic action, Sov. Phys. JETP **24**, 1006 (1967).